Time reversal of the excitation wave form in a dissipative pattern-forming system

Jana Heuer, Thomas John, and Ralf Stannarius
Institut für Experimentelle Physik, Otto-von-Guericke-Universität Magdeburg, Universitätsplatz 2, D-39106 Magdeburg, Germany
(Received 19 May 2008; published 19 September 2008)

We discuss the consequences of time reversal of the excitation parameters on the stability of a periodically driven dynamic system. The example chosen, electrohydrodynamic convection of nematics, is a well-investigated dissipative pattern-forming system, usually driven with time-periodic external electric fields $E(t)$. The dynamic model that describes linear stability at onset can be represented by a set of two differential equations for the amplitudes of the dynamic variables. Floquet analysis reveals an astonishing dynamic property: Under time reversal of any periodic excitation function $E(t)$, the dynamic equations reproduce the same stability thresholds, pattern types, and critical pattern wavelengths, even when the dynamics of all involved system variables are essentially different for the excitations $E(t)$ and $E(-t)$. Experimental confirmation of these mathematical predictions is provided by the measurement of threshold curves and the analysis of the time-resolved optical characteristics of the convection roll patterns.

DOI: 10.1103/PhysRevE.78.036218 PACS number(s): 05.45.−a, 47.54.−r, 61.30.−v

I. INTRODUCTION

Nematic electrohydrodynamic convection (EHC) is, besides e.g., Rayleigh-Bénard convection, Taylor vortices, or Faraday waves, among the most comprehensively investigated standard systems in dissipative pattern formation. Since periodic driving of EHC with arbitrarily synthesized wave forms of the electric field is conveniently manageable, this dynamic system is well suited to test the effects of time symmetries of the excitation in a parametrically driven dynamic system.

The phenomenon of EHC was first observed about four decades ago, independently, by Williams and Kapustin [1]. Certain nematic liquid crystals, exposed to an electric field in a thin sandwich cell, develop regular convection rolls. These are visible in transmitted light due to the periodic deflection of the optic axis (director). A model for the instability was proposed later by Carr [2] and Helfrich [3]. Theoretical understanding has developed considerably since then [4–15] (see, e.g., reviews in [13–16]). Extending the classical description of the patterns, flexoelectricity [17] and ionic charge dissociation-recombination processes [7,8] have been included in recent theories.

Contemporary nonlinear models can describe the different three-dimensional spatial patterns of normal, oblique, and abnormal rolls, with their particular wave-vector orientations respective to the preferential director axis, and they provide an understanding of higher instabilities like, e.g., chevron formation [10,18]. Electrical excitation is usually performed with ac fields; classically, one uses simple sine or square waves. The system response is time periodic of the same period as the excitation in these cases. The time dependence of the dynamic system variables (velocity, director, and charge fields) can be of different types. Two fundamental dynamic regimes, the conduction regime at low-frequency excitation and the dielectric regime at high excitation frequencies (separated by some cutoff frequency), have been distinguished early by the time symmetries of the system variables.

Recently, experiments have been performed with other periodic excitation wave forms that lack the high symmetries of simple sine or square waves. It has been demonstrated that in these situations, subharmonic EHC patterns exist [19–21]. Director, charge, and velocity fields are periodic with $2T$ in these structures when excitation has the period T. In an earlier study [21], we analyzed the conditions for the occurrence of subharmonic dynamics. In the formation of subharmonic patterns, the time symmetries of the excitation $E(t)$ play an important role. Three conditions have been formulated for the excitation sequence that are incompatible with subharmonic (T-antiperiodic) pattern dynamics. They exclude subharmonic patterns at simple sine- or square-wave excitations [21].

In dynamical systems where the equations are symmetric under time reversal (see, e.g., [22] and references therein), the reversal of a periodic variation of the system parameters has no qualitative consequences for the system dynamics—e.g., for the stability of certain solutions. However, for a large class of dynamic systems, in particular for systems that involve dissipation like the damped pendulum, time-reversal symmetry is broken in the dynamic equations. EHC belongs to this class. In this study, we focus on EHC driven with periodic wave forms of the electric field, $E(t)=E(t+T)$, which are asymmetric under time reversal. Among these wave forms, the simplest ones can be constructed by superposition of two or more rectangular waves. The dynamic variables will respond in a specific way to an excitation $E(t)$. It is evident that if the system is driven with the function $E(-t)$, the dynamic equations will in general lead to different trajectories of all the dynamic system variables. We demonstrate analytically that irrespective of the different dynamics during the excitation period, the mathematical model predicts the same threshold fields and the same structure of the stability diagram, including the existence ranges of the dynamic regimes of conduction, dielectric, and subharmonic patterns, for the forward and backward excitation sequences $E(t)$ and $E(-t)$. Experimental investigations of the threshold curves and of the dynamic properties of the optical patterns confirm these mathematical predictions.

This paper is structured as follows: we give a short recollection of the structure of the model equations in the following section and introduce the Floquet analysis of these equa-

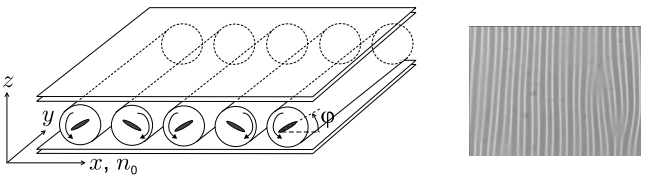

FIG. 1. Sketch of the cell geometry and normal convection rolls (left); the velocity (arrows) and director fields (rods) are indicated, and the coordinate system, the director deflection amplitude φ, and the director easy axis $\mathbf{n}_0$ are defined. Right: image of the convection rolls under transmission in the z direction and conduction regime. Picture dimensions are 355 μm $\times$ 265 μm.

tions in Sec. II A. In Sec. II B, we show analytically that the thresholds and neutral curves are reproduced under time reversal of the excitation. In the following section II C we present a numerical calculation of the trajectories of the system variables and show that these trajectories can be essentially different, irrespective of the identical stability thresholds, when the excitation lacks the necessary inversion symmetries. In Sec. III, experimental results obtained with a light-scattering technique are reported and compared to the model predictions. In the last section some conclusions and possible generalizations are discussed.

II. THEORETICAL MODEL

We describe the fundamental dynamics of the nematic electroconvection patterns near the onset of instability by a simple linearized differential equation system for two coupled system variables: the space-charge density $\tilde{q}$ and the director deflection $\tilde{\varphi}$ in the cell. At low flow field amplitudes, where inertia effects can be neglected, the flow field is directly coupled to the director field, so that director deflection and flow amplitudes are linearly related to each other.

The relevant Maxwell, Navier-Stokes, and torque balance equations in a two-dimensional description (normal rolls, wave vector along the director easy axis $\mathbf{n}_0$ as in Fig. 1) are linearized and condensed into a two-variable model. The director, flow, and charge fields are uniform in the direction y normal to the ground-state director. The director and flow fields have components only in the tilt plane formed by the preferential director alignment axis x and the cell normal z. The merits and shortcomings of this simplified description have been discussed in [21]. Experiments [19,20] have shown that it can reproduce the experimental observations, including the director field dynamics within each excitation cycle, with satisfactory accuracy. We use this model here, irrespective of its simplifications, to demonstrate the principal mechanism of the observed time-reversion invariance of the stability diagram.

A. Dynamic model equations and Floquet analysis

For the electric charge density $\tilde{q}(\vec{r},t)$ and the director deflection respective to the x axis, $\tilde{\varphi}(\vec{r},t)$, we employ a test-mode ansatz which separates the spatial modulation from the time-dependent amplitudes q and φ:

$$\tilde{q}(x,z,t) = q(t)\sin(k_x x)\cos(k_z z),$$

$$\tilde{\varphi}(x,z,t) = \varphi(t)\cos(k_x x)\cos(k_z z), \tag{1}$$

where $k_x = 2\pi/\lambda$ is the wave number of the test mode and λ is the lateral periodicity of the director, charge, and velocity fields. d is the cell thickness, and $k_z = \pi/d$. Of course, more sophisticated test functions may be introduced, which in particular match the boundary conditions for the flow field at the glass plates in a more realistic way. However, since this study is concerned mainly with the time symmetries of the resulting patterns instead of the details of the spatial structures, we sacrifice such complications for the sake of simplicity of the mathematical treatment.

The following approach is based on the ordinary differential equations (ODE) system introduced in [23] and follows essentially the lines of Ref. [21]. The time evolution of the amplitudes $\varphi(t)$ and $q(t)$ is described by two coupled ODEs, which are linear in φ and q:

$$\frac{d}{dt}\vec{Z}(t) = \mathbf{A}(t)\vec{Z}(t), \tag{2}$$

where

$$\vec{Z}(t) = \begin{pmatrix} q(t) \\ \varphi(t) \end{pmatrix}, \quad \mathbf{A}(t) = \begin{pmatrix} A_1 & A_2 E(t) \\ A_3 E(t) & A_4 + A_5 E^2(t) \end{pmatrix}.$$

The coefficients A_i contain material and cell parameters as well as wave numbers of the test modes (see the Appendix of [21]) so that the time dependence of $\mathbf{A}$ is contained in the coefficients $E(t)$ alone. $E(t) = U(t)/d$ is the electric field strength, related to the voltage $U(t)$ applied to the cell. When the electric field is time periodic with period T, $E(t) = E(t+T)$; the same applies to the components of the matrix $\mathbf{A}$, $\mathbf{A}(t) = \mathbf{A}(t+T)$. This case will be treated in the following.

Floquet analysis has been used as a successful tool for the construction of the stability diagram of the convection patterns. The fundamental solution of the ODE system (2) can be written as

$$\vec{Z}(t) = \mathbf{P}(t)\vec{Z}(0), \tag{3}$$

where the evolution matrix $\mathbf{P}(t)$ fulfills the equation $\dot{\mathbf{P}}(t) = \mathbf{A}(t)\mathbf{P}(t)$ and $\mathbf{P}(0) = \mathbf{E}$ is the unit matrix. The Floquet theorem predicts that $\mathbf{P}$ can be written in a form $\mathbf{P}(t+T) = \mathbf{P}(t)\mathbf{M}$. The regular transfer matrix $\mathbf{M}$ with eigenvalues μ_1 and μ_2 (the Floquet multipliers) determines the evolution of the dynamic variables after one full excitation period. The stability threshold is found from the condition that the Floquet multiplier μ_1 with the largest absolute value matches $|\mu_1| = 1$. The ground state $\vec{Z} = (0,0)$ is stable as long as $1 > |\mu_1| > |\mu_2|$. In general, there is no straightforward relation between the elements of $\mathbf{A}(t)$ and the Floquet multipliers [24]. For homogeneous ODE systems like Eq. (2), one has [25]

$$\mu_1\mu_2 = \det(\mathbf{M}) = \exp\left(\int_0^T \mathrm{Tr}\mathbf{A}(t)dt\right). \quad (4)$$

In the standard EHC model, all coefficients in the matrix $\mathbf{A}(t)$ are real. Consequently, the exponential in Eq. (4) is positive and the product $\mu_1\mu_2$ as well. The real parts of the Floquet multipliers have the same sign; μ_1 and μ_2 are either both real or complex conjugated.

The strategy for the stability test of the ground state $\vec{Z}(t)=(0,0)$ is the following: in the case of simple square-wave or sine-wave excitation, we parametrize the excitation wave form with the excitation period $T=1/f$ and the excitation amplitude E_0. Then we consider test modes according to Eqs. (1) with wave number k_x and calculate the Floquet multipliers for fixed excitation frequencies f and given shapes of the excitation wave forms, using $U_0=E_0d$ and k_x as parameters. The condition $|\mu_1|=1$ defines the segments of the neutral curve in the two-dimensional amplitude–wave-number (U_0,k_x) plane. We determine the global minimum of U_0 on this neutral curve, which gives the onset threshold of EHC for the given wave form and frequency. From a set of such minima of neutral curves for different excitation frequencies, the threshold curves for the conduction, dielectric, and subharmonic regimes can be constructed [19–21]. Alternatively, in this paper we fix the frequencies of two superimposed wave components (see below) and use the amplitudes of these components as parameters to construct pattern state diagrams.

In all situations studied here, the μ_i are real in the vicinity of the neutral curves.[1] When near the minimum of the neutral curve both μ_i are positive, the system has T-periodic solutions for the given excitation frequency, corresponding to either the conduction or dielectric regimes. When the two μ_i are negative near the minimum of the neutral curve, the system has T-antiperiodic (subharmonic) solutions [19].

B. Time-reversal and stability thresholds

In order to show mathematically straightforwardly that the thresholds and critical wave numbers for any given excitation $E(t)$ coincide with those of the time-reversed excitation $E(-t)$, we follow the approach of our earlier study and exploit the property that the off-diagonal elements of $\mathbf{A}(t)$, a_{12}, and a_{21} have the same dependence on $E(t)$, except for a constant factor. This condition is sufficient but not necessary for the above-mentioned property. We symmetrize $\mathbf{A}$ by introducing the dimensionless dynamic variable

$$\hat{q}(t) = \sqrt{a_{21}/a_{12}}q(t) = \sqrt{A_3/A_2}q(t)$$

(the caret is dropped for simplicity in the following) and set $a=\sqrt{a_{21}a_{12}}\,\mathrm{sign}(E)=\sqrt{A_2A_3}E$:

$$\mathbf{A}(t) = \begin{pmatrix} a_{11}(t) & a(t) \\ a(t) & a_{22}(t) \end{pmatrix}.$$

The full excitation period is split into equidistant, infinitesimally small time intervals $\delta t=t_{i+1}-t_i=T/N$, in which $\mathbf{A}$ can be approximated as constant. Then one can integrate the ODE system with constant coefficients in each of these intervals,

$$\vec{Z}(t_{i+1}) = \mathbf{P}_i\vec{Z}(t_i),$$

with $\mathbf{P}_i=\exp[\mathbf{A}(t_i)\delta t]$.

The fundamental solution for the full excitation period, $\vec{Z}(T)=\mathbf{P}\vec{Z}(0)$, is calculated by the product of the $\mathbf{P}_i$ of all N infinitesimal intervals:

$$\mathbf{P} = \lim_{N\to\infty} \prod_{i=0}^{N-1} \mathbf{P}_{N-i},$$

where $\delta t=T/N\to 0$.

For an excitation wave form that is derived from $E(t)$ by time reversal, we can calculate $\vec{Z}(T)$ from $\vec{Z}(0)$ by the same approach, but replace all $\mathbf{A}(t_i)$ by $\mathbf{A}(T-t_i)$ and thus also $\mathbf{P}(t_i)$ by $\mathbf{P}(T-t_i)$. The matrices $\mathbf{P}_i$ have to be multiplied in reverse order to yield a solution of the form $\vec{Z}(T)=\mathbf{P}_{(\mathrm{rev})}\vec{Z}(0)$:

$$\mathbf{P}_{(\mathrm{rev})} = \lim_{N\to\infty} \prod_{i=1}^{N} \mathbf{P}_i.$$

Products of N matrices $\mathbf{P}_i$ have the general property

$$\left\{\prod_{i=1}^{N} \mathbf{P}_i\right\}^{\mathrm{T}} = \prod_{i=0}^{N-1} \mathbf{P}_{N-i}^{\mathrm{T}},$$

and from $\mathbf{P}_i=\mathbf{P}_i^{\mathrm{T}}$ it follows that $\mathbf{P}_{(\mathrm{rev})}=\mathbf{P}^{\mathrm{T}}$; i.e., the fundamental matrices for the two wave forms are transposed matrices of each other. Consequently, the characteristic multipliers for any excitation wave form and its time-reversed counterpart are identical, irrespective of material and geometrical parameters contained in $\mathbf{A}$.

All neutral curves and thresholds, including the temporal periodicities of the convection patterns at onset, are the same for such pairs of time-mirrored excitation wave forms. In the physical system, we predict that any two time-mirrored excitation sequences lead to identical threshold voltages, identical wave vectors, and identical pattern regimes (conduction, subharmonic, or dielectric).

On the other hand, there are only a few special time-mirrored wave forms that reproduce exactly the same trajectories of the dynamic variables under time reversal. Among those are wave forms that are symmetric under time reversal—e.g., simple harmonic and square-wave functions—where $E(t_0+t)=E(t_0-t)$ for a certain t_0. It is trivial that they lead to identical thresholds. Wave forms that are antisymmetric under time reversal, $E(t_0+t)=-E(t_0-t)$—e.g., triangular and sawtooth functions—produce trajectories of the dynamic variables that differ from their counterparts only by the signs, so it is trivial again that the same thresholds and patterns are found. In general, however, any other wave form leads to trajectories of the dy-

[1] It has been discussed in Ref. [21] that in the particular system considered here ($\varepsilon_a=\varepsilon_\parallel-\varepsilon_\perp<0$), $\mathrm{Tr}(\mathbf{A})$ is always negative, and thus Eq. (4) requires that $\mu_1\mu_2<1$. If the μ_i are complex conjugated, their absolute values are smaller than 1.

namic variables that differ from their counterparts under time-reversed excitation. In these cases, it is mathematically obvious, but not evident *a priori* in the physical system that the thresholds and all other properties of the patterns (wavelengths, orientations) except the individual trajectories of the system variables, coincide exactly.

C. Numerical results

Analytical trajectories of the system variables $q(t)$ and $\varphi(t)$ can be calculated only in few special situations—in particular, for wave forms composed of piecewise constant segments. In this section, we solve the equations for a couple of exemplary wave forms. Although this can be achieved analytically for the superimposed square waves considered here, we have chosen a numerical approach for convenience. We note that the analytical derivation in the previous section is general for all wave forms. Here, it may suffice for a demonstration to show one example of a wave form that produces an identical pattern stability diagram to its time-reversed counterpart.

For the construction of the following stability diagrams, the wave number and the amplitudes of the superimposed electric field components are varied systematically. For each parameter set, two independent initial vectors $\vec{Z}_1(0)$ and $\vec{Z}_2(0)$ are chosen, and their evolution is calculated for a full excitation period by solving Eq. (2). From the values $Z_1(T)$ and $Z_2(T)$, the elements of $\mathbf{M}$ are obtained.

In the numerical calculations, we refer to the data of the nematic material *Mischung 5* [19–21], which has been used in the experiments. We assume $\sigma_\parallel = 320\ \mathrm{s}^{-1}$ (cgs), $\sigma_\perp = 213\ \mathrm{s}^{-1}$ (cgs), $\gamma_1 = 3.78\ \mathrm{g\ cm}^{-1}\ \mathrm{s}^{-1}$ (cgs), $\varepsilon_\parallel = 5.6$, $\varepsilon_\perp = 6.0$, and a cell thickness of $d = 20.2\ \mu\mathrm{m}$.

The wave forms considered here are superpositions of two rectangular waves with amplitudes E_1 and E_2,

$$E(t) = E_1\ \mathrm{sgn}\left(\sin\frac{2\pi t}{T_1}\right) + E_2\ \mathrm{sgn}\left(\sin\frac{2\pi(t+\delta)}{T_2}\right),$$

and the time-reversed functions $E(-t)$. The frequency ratio between the two components is chosen as 1:4—i.e., $T_1 = 4T_2$. The amplitudes of the two components are varied as parameters while the periods are fixed. In order to obtain patterns in all three dynamic regimes, we choose the two frequencies such that one of them is below and the second one is above the cutoff frequency that discriminates conduction and dielectric regimes for simple square waves—i.e., $T_1 = 10$ ms and $T_2 = 2.5$ ms. The time shift δ defines a delay between the two wave components, expressed as a phase shift θ of the faster frequency respective to the slower one by $\theta = 2\pi\delta/T_2$. As discussed earlier [21], a subharmonic regime can appear between the conduction and dielectric regimes when $\theta \neq n\pi/2$, $(n = 1, 2, \ldots)$. Figure 2 sketches the excitation wave forms. This excitation is symmetric under time reversion for $\theta = 90°$; it is antisymmetric for $\theta = 0°$ and asymmetric for any other phase shifts between $0 < \theta < 90°$.

The Floquet multiplier μ_1 is obtained as a function of the test-mode wave number and either electric field strength parameter. The numerical approach does not only confirm the analytical predictions of the previous section. We also obtain the trajectories of the dynamic variables for special wave forms. One of the variables, the director deflection amplitude, is related to observables in the experiment, both to the optical texture amplitude in transmission and to the scattering efficiency of the grating formed by the regular director pattern. It can be compared with experimental data of the time-dependent intensity of laser-scattering reflexes that are presented in the next section.

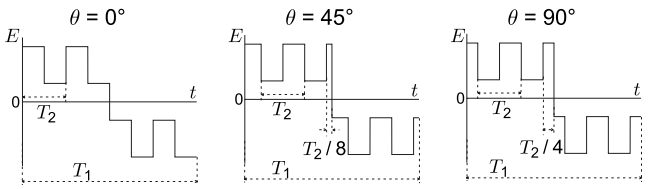

FIG. 2. Superposition of rectangular wave forms in this experiment (schematic). Left: time-reversion-antisymmetric wave form, $\theta = 0°$. Middle: time-asymmetric wave form, $\theta = 45°$. Right: time-reversion-symmetric wave form, $\theta = 90°$. The frequency ratio is 1:4.

In Fig. 3, both dynamic variables $\varphi(t)$ and $q(t)$ are presented exemplarily for the excitation $E(t)$ with $\theta = 0°$ in the conduction regime.

Figures 4 and 5 show trajectories in the (φ, q) phase space for exemplary excitation parameters. The time-reversion-symmetric excitation ($\theta = 90°$, bottom) yields equivalent trajectories of the system variables for the forward- and backward-excitation sequences. Note that each solution $(\varphi(t), q(t))$ is equivalent to $(-\varphi(t), -q(t))$, which corresponds to a constant global shift of the pattern by a half spatial period, π/k_x. In the time-reversion-antisymmetric excitation wave form ($\theta = 0°$), the backward-excitation sequence corresponds to a sign inversion of E. Thus, one has to change the sign of one of the dynamic variables in the solutions of the forward sequence; i.e., in the phase space in Figs. 4 and 5, the two trajectories for the forward- and backward-excitation

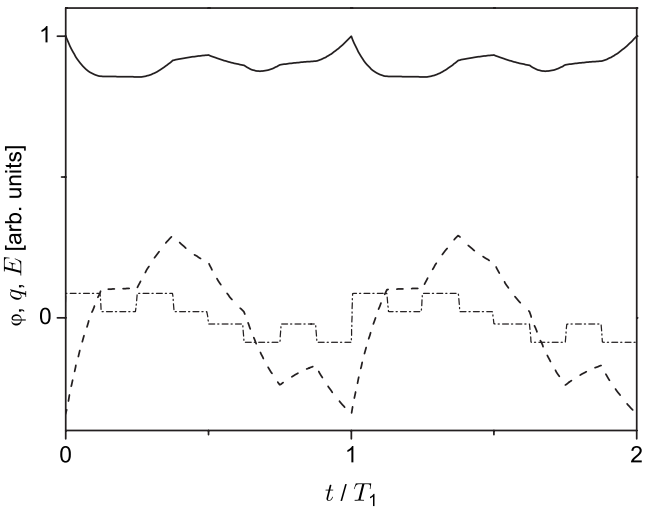

FIG. 3. Calculated time dependence of φ (solid line) and q (dashed line) for the excitation E (dash-dotted line) with $\theta = 0$, near the threshold in the conduction regime. The curves belong to the trajectory in Fig. 4, top left. $U_{\mathrm{high}} = 10.1$ V.

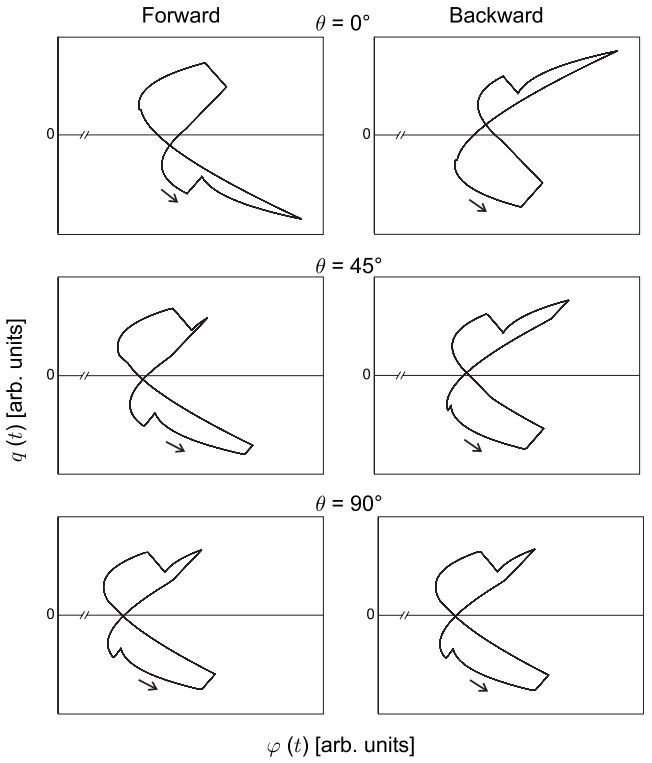

FIG. 4. Trajectories of the amplitudes $\varphi(t)$ and $q(t)$ of the director deflection and charge density in the phase space (φ,q) near threshold in the conduction regime. The excitation wave forms at $\theta=0°$ (top) and $\theta=90°$ (bottom) are antisymmetric and symmetric, respectively, under time reversion; consequently, the trajectories of the dynamic variables are either identical or simply mirrored at one of the coordinate axes. The asymmetric excitation for $\theta=45°$ (middle) yields completely different trajectories for the forward- and backward-excitation wave forms. Arrows indicate the sense of the orbits. $U_{\text{high}}=10.1$ V.

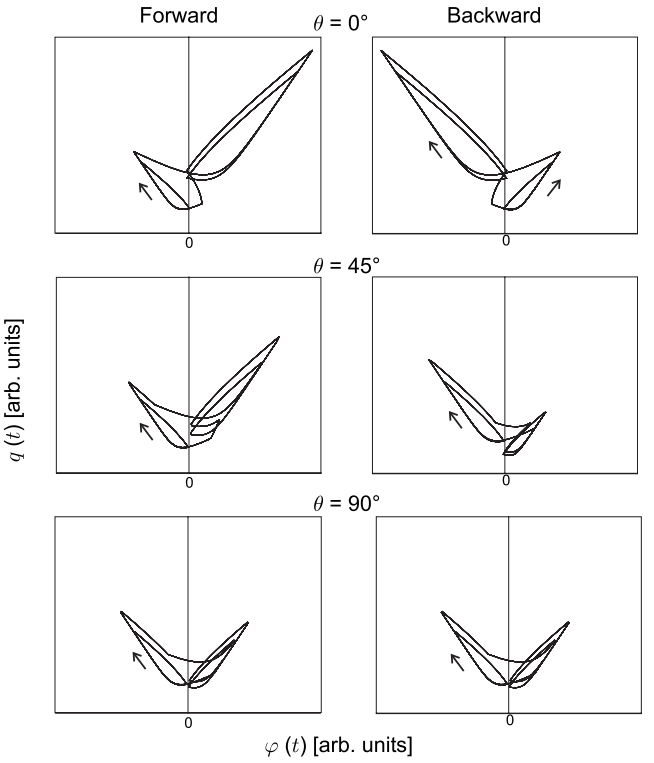

FIG. 5. Same as previous image for patterns in the dielectric regime. The time-antisymmetric excitations with $\theta=0°$ yield trajectories that are mirrored at one of the axes, the time-symmetric excitations with $\theta=90°$ yield trajectories that are identical, and the trajectories for the asymmetric excitations $\theta=45°$ are well distinguishable. Arrows indicate the sense of the orbits. $U_{\text{high}}=47.9$ V.

wave forms are mirrored at one of the coordinate axes. Obviously, the dynamics must otherwise be identical and thus thresholds and critical wave numbers coincide.

When the phase shift is continuously increased from 0° to 90°, there is a gradual transition from the situation where $E(t)$ and $E(-t)$ produce mirror-symmetric trajectories to that where $E(t)$ and $E(-t)$ produce the same trajectories. At intermediate phase shifts θ, the trajectories for forward and backward excitation increasingly differ from each other; representative data are shown for the asymmetric wave forms of $\theta=45°$ (Figs. 4 and 5, middle) where the difference between both trajectories is maximum. The two trajectories are obviously different and cannot be mapped onto each other by simple coordinate transformations. Irrespective of that, the analytical result that the neutral curves in the stability diagram coincide for forward- and backward-excitation sequences is confirmed by the numerical results. More numerical results are presented in the next section in the context of the respective experimental data.

The $q(\varphi)$ trajectories for the forward- and backward-excitation wave form with parameters that yield subharmonic dynamics are depicted in Fig. 6. An asymmetric wave form with $\theta=15°$ is chosen here. The subharmonic pattern regime vanishes at higher phase shifts θ. In order to accentuate the difference between both trajectories, the curve generated by the backward excitation has been mirrored at the $q=0$ axis. As analyzed earlier [21], the subharmonic trajectories cover all four quadrants of the (φ,q) phase space, in contrast to the conduction and dielectric regimes.

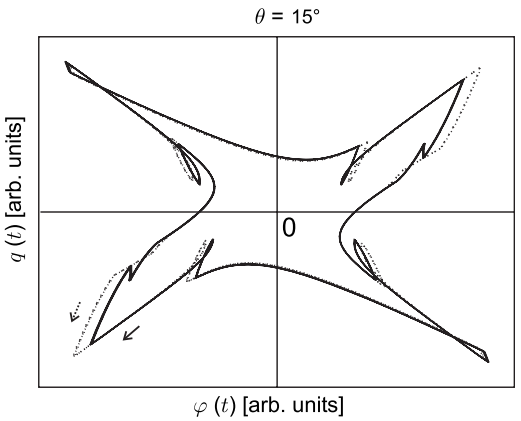

FIG. 6. $q(\varphi)$ trajectories in the subharmonic regime with $\theta=15°$ near threshold. The trajectory belonging to the backward excitation (dotted line) has been mirrored at the $q=0$ axis for comparison with the forward case (solid line). Arrows indicate the temporal direction. $U_{\text{high}}=35.9$ V.

III. EXPERIMENT

The experiment is performed in a 20.2-μm-thick commercial sandwich cell. Rubbed polyimide layers provide planar surface alignment of the director; transparent indium-tin-oxide (ITO) electrodes are used for the electric field, which is generated by a Labview controlled function generator (Agilent 33220A) and amplified by a linear amplifier. The cell is illuminated by a He-Ne laser, and the scattering peak corresponding to the first harmonic of the spatial pattern period is recorded as a function of time with a photodiode [19,20]. The relation between scattering profiles and director deflections is described, e.g., in [26–29].

Figure 7 compares pattern-state diagrams corresponding to forward and backward excitations for different parameter sets. As parameters, we have chosen the amplitudes of the two superimposed square waves at fixed frequencies. Since the two frequencies components are chosen on opposite sides of the cutoff frequency, the intersection of the onset threshold curve with the abscissa (high-frequency component) gives the onset voltage for dielectric rolls at 400 Hz and the intersection with the ordinate (low-frequency component) gives the onset threshold of conductive rolls at 100 Hz. In order to construct the stability diagram, the amplitude of the fast, 400-Hz component, $U_{\text{high}}=E_2 d$ (indices high and low refer to the frequency), is fixed and the amplitude of the 100-Hz component, $U_{\text{low}}=E_1 d$, is increased from zero to the threshold. Then, the value is marked and the next U_{high} value is chosen. In the case of large U_{high}, U_{high} is varied at fixed U_{low}. As expected, the measured thresholds in the top picture (symbols), for $\theta=0°$, are identical within experimental resolution. The same applies for $\theta=90°$. This follows from the symmetries of the excitation sequences. More important, the diagram in Fig. 7 (center) shows that the thresholds also coincide if the excitation sequence is time asymmetric. In addition to the threshold data, it is evident that the pattern wave numbers at onset coincide as well for all parameter combinations and all dynamic regimes. Since the scattering reflexes do not contain information on the spatial phase of the pattern, we have checked and verified by conventional polarizing microscopy that the patterns are stationary at onset. This justifies that we can neglect weak electrolyte effects in the model.

Figure 7 also shows the calculated threshold voltages determined from the global minima of the neutral curves in the U_{low}, k_x parameter space at fixed U_{high} (solid lines). One can see that for all three excitation wave forms the general appearance of the stability diagrams is reproduced. Both threshold fields and critical wave numbers obey the correct trends; they are quantitatively correct, and the transitions between conduction, subharmonic, and dielectric regimes are well reproduced. In the region of high U_{high} values, within the dielectric regime, there is an apparent mismatch between calculated and measured thresholds in all cases. This may be attributed to the oversimplified choice of test functions in the case of dielectric convection structures.

Figures 8–10 compare the intensity change of the laser scattering intensity at the first-order reflex for forward- and backward-excitation wave forms and the calculated trajectories of the director deflection amplitudes for both excitations.

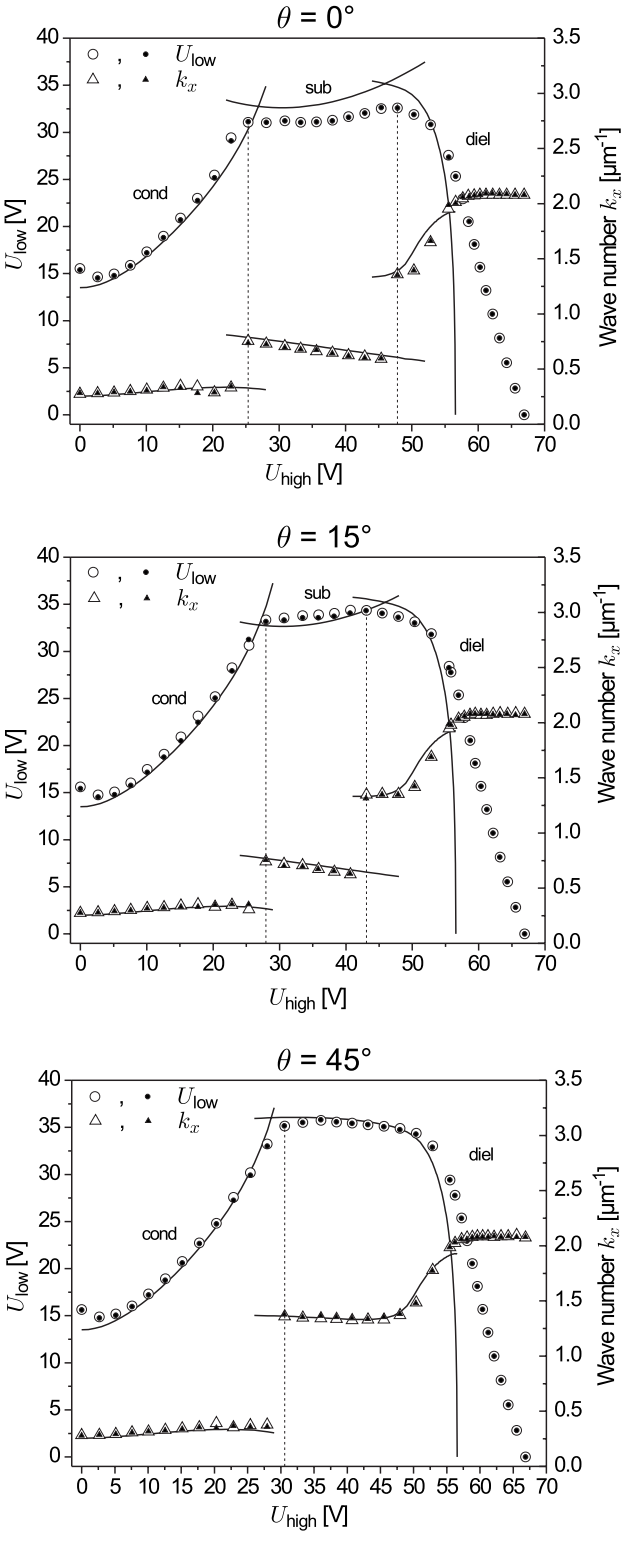

FIG. 7. Measured (symbols) stability diagrams for superimposed square-wave excitation. Threshold fields for forward- (open symbols) and backward- (solid symbols) excitation sequences coincide for all parameter choices, $\theta=0°$ (top), $\theta=15°$ (center), and $\theta=45°$ (bottom). Frequencies are 100 Hz and 400 Hz for U_{low} and U_{high}, respectively. The transitions between measured conduction (cond), subharmonic (sub), and dielectric (diel) regimes are marked by dotted lines. Solid lines show calculated thresholds and wave numbers; forward and backward excitations are identical.

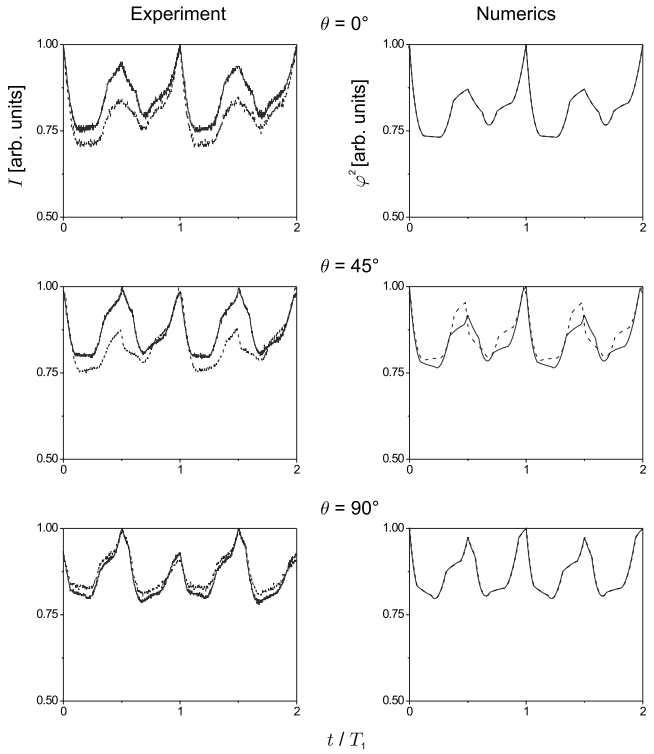

FIG. 8. Comparison of the numerically calculated trajectories of $\varphi^2(t)$ for a forward- (solid line) and backward- (dashed line) excitation sequence and the experimentally determined laser-scattering intensities $I(t)$ of the first-order reflex for both sequences in the conduction regime. The trajectories of $\varphi(t)$ do not have zeros, but the intensity varies during the excitation period. $U_{\text{high}}=10.1$ V like in Fig. 4.

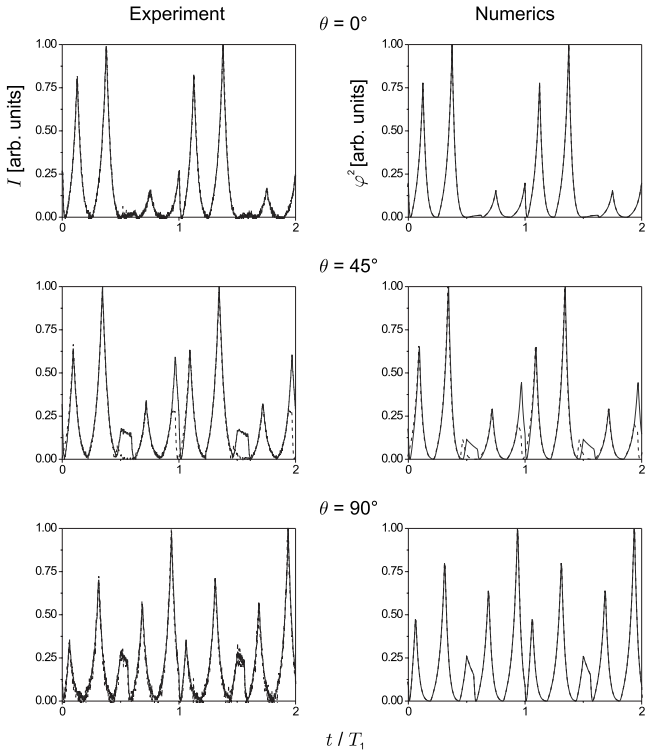

FIG. 9. Same as previous image for the dielectric regime. The trajectories of $\varphi(t)$ pass zero at least twice in each excitation cycle. $U_{\text{high}}=47.9$ V like in Fig. 5.

We present the square of the calculated deflection amplitude φ, which is in first approximation proportional to the scattering intensity, if the light beams are deflected in the nematic layer (amplitude grid). With this approximation, the general shapes and peak positions of the experimental $I(t)$ curve are well reproduced for all parameters; the intensities of the peaks may differ somewhat.

The important result is that for the time-reversal antisymmetric and symmetric wave forms ($\theta=0°$ and $\theta=90°$ in Figs. 8 and 9), the calculated graphs for forward- and backward-excitation sequences are identical. The same applies for the experimental curves, except for some mismatch in absolute intensity in the 0° curves. The reason for this mismatch is probably found in a very small dc offset of the synthesized wave forms. Such an offset influences the two symmetric wave forms (90°) in the same way. For antisymmetric wave forms (0°), it leads to slightly different trajectories in the case of conduction patterns (not in the dielectric case where the director oscillates with the excitation period T).

The trajectories for the asymmetric wave form with $\theta=45°$ and its time-mirrored counterpart differ in both regimes. Figure 10 shows the results for $\theta=15°$ in the subharmonic regime (which is absent at $\theta=45°$). These experimental data confirm the calculated results.

The gradual transformation of the measured amplitude dynamics for forward and backward excitation from $\theta=0°$ $[E(t)=-E(-t)]$ to $\theta=45°$ $[E(t)\neq -E(-t)]$ is depicted in Fig. 11. While the intensity characteristics is identical at $\theta=0°$, the $I(t)$ curves generated by forward and backward excitation differ increasingly with higher θ; they are most distinguishable at $\theta=45°$.

IV. CONCLUSIONS

It has been shown here by analytical investigation of the dynamic equations in standard electrohydrodynamic convection that any periodic excitation $E(t)$ produces the same threshold fields and critical wave numbers as the excitation $E(-t)$, irrespective of the time-reversal symmetry properties of $E(t)$. We have further shown exemplarily by numerical calculations that there are time-reversal asymmetric wave

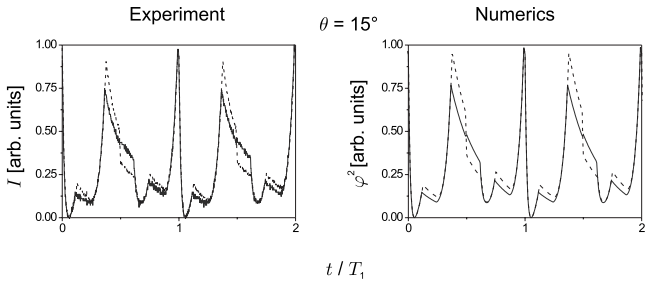

FIG. 10. Calculated trajectories of $\varphi^2(t)$ and measured intensity I in the subharmonic regime for forward- (solid) and backward- (dashed) excitation sequences. The trajectories of $\varphi(t)$ pass zero once in each excitation cycle; thus, φ^2 touches the abscissa once in each period. $U_{\text{high}}=35.9$ V like in Fig. 6.

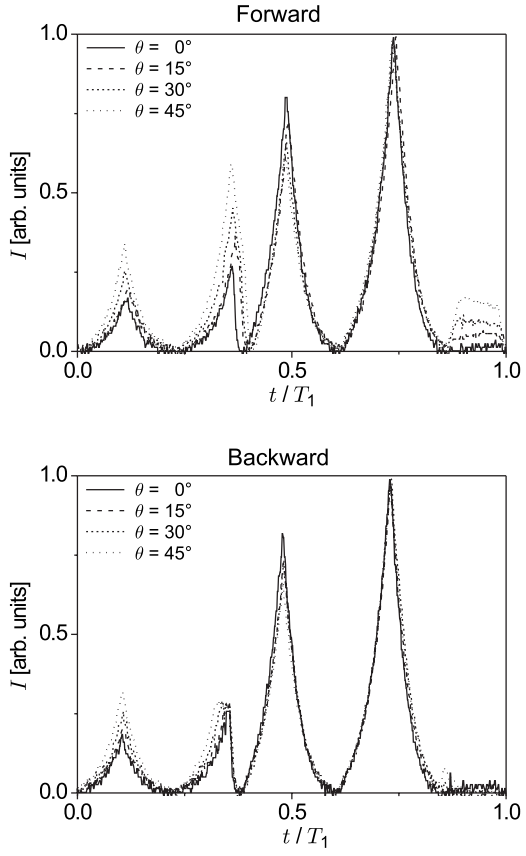

FIG. 11. Experimentally determined laser-scattering intensity I of the first-order reflex in the dielectric regime for various θ. While the trajectories are identical for forward and backward excitation at θ=0° (solid line), they differ the strongest for θ=45° (dotted line). U_{high}=47.9 V.

forms that produce different trajectories of the system variables for the forward- and backward-excitation sequences, while, in agreement with the analytical result, yielding identical thresholds and critical wave numbers. Finally, experiments have been performed with a nematic mixture in a planar sandwich cell that show the same qualitative results. Within experimental accuracy, threshold fields and pattern wavelengths coincide for any tested forward- and backward-excitation sequences. The dynamics of the director deflection for the forward- and backward-excitation sequences can be well distinguished if the excitation lacks time-reversal symmetry. Time reversal of the excitation wave form in nematic electroconvection leaves all properties of the spontaneously formed dissipative spatiotemporal patterns at onset preserved, except for the trajectories of the system variables during each excitation cycle.

In the numerical calculations, we have chosen piecewise constant excitation functions in order to keep the numerical efforts small. The analytical result, however, holds for general wave forms. The same results can be expected for excitation, e.g., with certain types of sawtooth wave forms or any superposition of harmonic functions.

These dynamic properties of the EHC model equations, derived analytically in Sec. II B, can probably be generalized to some other dynamic systems described by two dynamic variables. The sufficient condition in our analytical approach is that the differential equation system can be symmetrized in the off-diagonal elements of the propagator matrix, but this condition is not necessary. The observed phenomenon is more general and its occurrence in other dynamic systems may deserve further investigation. Other pattern-forming systems like Faraday waves also involve a time-periodic excitation (see, e.g., reviews in [30,31]). Classically, this system is driven with sinusoidal waves that are invariant under time reversal, but in principle, arbitrary driving wave forms can be applied to test the invariance of the stability thresholds in this system [32]. Even Rayleigh-Bénard convection, which is classically driven with a constant control parameter, can be studied under periodically modulated thermal gradients [33] or variable gravitational acceleration [34,35]. Another example is Taylor-Couette vortices. They are usually observed at constant rotation speed of the cylinders, but have been studied under periodically modulated excitations as well (e.g., [36,37]). For none of these systems, the question has been analyzed so far whether a time reversal of the excitation function leads to a change of the pattern stability diagram.

We note that the preservation of the stability thresholds under time reversal of the driving parameters is trivial only for one-dimensional systems. In two or higher dimensions, the result would be trivial only if the matrices $\mathbf{A}(t)$ for different times t_1 and t_2 commute. In that case, the solution of the differential equation system can be written as an exponential of the time integral of $\mathbf{A}(t)$. Here we may restrict ourselves to one short remark: Commuting matrices $\mathbf{A}(t_1)$ and $\mathbf{A}(t_2)$ for any t_1 and t_2 mean that any time intervals of the excitation sequence can be interchanged, or resorted, without influence on the Floquet multipliers and system stability. This is in general not the case in dynamical systems. In the EHC model equations, in particular, the matrices $\mathbf{A}(t)$ do not commute at arbitrary times $t_1 \neq t_2$, but nevertheless the system shows the above-described coincidence of stability thresholds because of the symmetry of the off-diagonal elements. It is easy to show that there are periodically driven two-dimensional linear dynamic systems—for example, the parametrically excited pendulum—where time reversal of the periodic driving leads to both different trajectories *and* different stability thresholds, so the described property is rather unique. At present, we do not see a general criterion for a decision whether a time reversal of multiplicative excitation parameters in a certain dynamic system will lead to identical thresholds in the stability diagrams.

ACKNOWLEDGMENTS

One of the authors (J.H.) has been supported by the Landesstipendium Sachsen-Anhalt. Andreas Engel is acknowledged for valuable discussions.

[1] R. Williams, J. Chem. Phys. **39**, 384 (1963); A. P. Kapustin and L. K. Vistin, Kristallografiya **10**, 118 (1965).
[2] E. F. Carr, J. Chem. Phys. **38**, 1536 (1963).
[3] W. Helfrich, J. Chem. Phys. **51**, 4092 (1969).
[4] W. Zimmermann and L. Kramer, Phys. Rev. Lett. **55**, 402 (1985).
[5] E. Bodenschatz, W. Zimmermann, and L. Kramer, J. Phys. (Paris) **49**, 1875 (1988).
[6] E. Plaut, W. Decker, A. G. Rossberg, L. Kramer, W. Pesch, A. Belaidi, and R. Ribotta, Phys. Rev. Lett. **79**, 2367 (1997).
[7] M. Treiber and L. Kramer, Mol. Cryst. Liq. Cryst. Sci. Technol., Sect. A **261**, 311 (1995).
[8] M. Dennin, M. Treiber, L. Kramer, G. Ahlers, and D. S. Cannell, Phys. Rev. Lett. **76**, 319 (1996).
[9] W. Zimmermann, in *Nematics Mathematical and Physical Aspects*, edited by J.-M. Coron, J.-M. Ghidaglia, and F. Hélein (Kluwer Academic, 1991), p. 401.
[10] A. G. Rossberg and L. Kramer, Physica D **115**, 19 (1998).
[11] L. Kramer, E. Bodenschatz, W. Pesch, W. Thom, and W. Zimmermann, Liq. Cryst. **5**, 699 (1989).
[12] Y. Tu, Phys. Rev. E **56**, R3765 (1997).
[13] W. Pesch and U. Behn, in *Evolution of Spontaneous Structures in Dissipative Continuous Systems*, edited by F. H. Busse and S. C. Müller (Springer, Heidelberg, 1998), p. 335.
[14] L. Kramer and W. Pesch, Annu. Rev. Fluid Mech. **27**, 515 (1995).
[15] L. Kramer and W. Pesch, in *Pattern Formation in Liquid Crystals*, edited by A. Buka and L. Kramer (Springer, New York, 1996), p. 221.
[16] A. Buka, N. Éber, W. Pesch, and L. Kramer, in *Self-Assembly, Pattern Formation and Growth Phenomena in Nano-Systems*, edited by A. A. Golovin and A. A. Nepomnyashchy (Springer, Berlin, 2006), p. 55.
[17] A. Krekhov, W. Pesch, N. Éber, T. Tóth-Katona, and Á. Buka, Phys. Rev. E **77**, 021705 (2008).
[18] H. Amm, R. Stannarius, and A. G. Rossberg, Physica D **126**, 171 (1999).
[19] Th. John and R. Stannarius, Phys. Rev. E **70**, 025202(R) (2004).
[20] Th. John, J. Heuer, and R. Stannarius, Phys. Rev. E **71**, 056307 (2005).
[21] R. Stannarius, J. Heuer, and T. John, Phys. Rev. E **72**, 066218 (2005).
[22] J. S. W. Lamb and J. A. G. Roberts, Physica D **112**, 1 (1998).
[23] U. Behn, A. Lange, and T. John, Phys. Rev. E **58**, 2047 (1998).
[24] E.g., I. J. Epstein, Proc. Am. Math. Soc. **13**, 690 (1962); J. Differ. Equations **1**, 206 (1965); J. S. Muldowney, Proc. Am. Math. Soc. **18**, 22 (1967).
[25] See, e.g., J. Hale, *Ordinary Differential Equations*, 2nd ed. (Krieger, Malabar, FL, 1980).
[26] J. A. Kosmopoulos and H. M. Zenginoglou, Appl. Opt. **26**, 1714 (1987).
[27] H. M. Zenginoglou and J. A. Kosmopoulos, Appl. Opt. **27**, 3898 (1988).
[28] T. John, U. Behn, and R. Stannarius, Eur. Phys. J. E **35**, 267 (2003).
[29] C. Bohley, J. Heuer, and R. Stannarius, J. Opt. Soc. Am. A **22**, 2818 (2005).
[30] J. Miles and D. Henderson, Annu. Rev. Fluid Mech. **22**, 143 (1990).
[31] H. W. Müller, R. Friedrich, and D. Papathanassiou, in *Lecture Notes in Physics*, edited by F. Busse and S. C. Müller (Springer, Berlin, 1998).
[32] W. S. Edwards and S. Fauve, J. Fluid Mech. **278**, 123 (1994).
[33] G. Ahlers, P. C. Hohenberg, and M. Lücke, Phys. Rev. Lett. **53**, 48 (1984).
[34] T. Boulal, S. Aniss, M. Belhaq, and R. Rand, Phys. Rev. E **76**, 056320 (2007).
[35] U. E. Volmar and H. W. Müller, Phys. Rev. E **56**, 5423 (1997).
[36] R. J. Donnelly, Proc. R. Soc. London, Ser. A **281**, 130 (1964).
[37] P. Riley and R. Laurence, J. Fluid Mech. **75**, 625 (1976).